The future of airborne sulfur-containing particles in the absence of fossil fuel sulfur dioxide emissions

Véronique Perraud[a], Jeremy R. Horne[b], Andrew S. Martinez[b,1], Jaroslaw Kalinowski[c,d], Simone Meinardi[a], Matthew L. Dawson[b], Lisa M. Wingen[a], Donald Dabdub[b], Donald R. Blake[a], R. Benny Gerber[a,c,d], and Barbara J. Finlayson-Pitts[a,2]

[a]Department of Chemistry, University of California Irvine, Irvine, CA 92697; [b]Department of Mechanical & Aerospace Engineering, University of California Irvine, Irvine, CA 92697; [c]Institute of Chemistry and the Fritz Haber Research Center, The Hebrew University of Jerusalem, Jerusalem 91904, Israel; and [d]Department of Chemistry, University of Helsinki, FIN-00014 Helsinki, Finland

Edited by Mark H. Thiemens, University of California at San Diego, La Jolla, CA, and approved September 23, 2015 (received for review June 1, 2015)

Sulfuric acid (H_2SO_4), formed from oxidation of sulfur dioxide (SO_2) emitted during fossil fuel combustion, is a major precursor of new airborne particles, which have well-documented detrimental effects on health, air quality, and climate. Another precursor is methanesulfonic acid (MSA), produced simultaneously with SO_2 during the atmospheric oxidation of organosulfur compounds (OSCs), such as dimethyl sulfide. In the present work, a multidisciplinary approach is used to examine how contributions of H_2SO_4 and MSA to particle formation will change in a large coastal urban area as anthropogenic fossil fuel emissions of SO_2 decline. The 3-dimensional University of California Irvine–California Institute of Technology airshed model is used to compare atmospheric concentrations of gas phase MSA, H_2SO_4, and SO_2 under current emissions of fossil fuel-associated SO_2 and a best-case futuristic scenario with zero fossil fuel sulfur emissions. Model additions include results from (*i*) quantum chemical calculations that clarify the previously uncertain gas phase mechanism of formation of MSA and (*ii*) a combination of published and experimental estimates of OSC emissions, such as those from marine, agricultural, and urban processes, which include pet waste and human breath. Results show that in the zero anthropogenic SO_2 emissions case, particle formation potential from H_2SO_4 will drop by about two orders of magnitude compared with the current situation. However, particles will continue to be generated from the oxidation of natural and anthropogenic sources of OSCs, with contributions from MSA and H_2SO_4 of a similar order of magnitude. This could be particularly important in agricultural areas where there are significant sources of OSCs.

methanesulfonic acid | sulfuric acid | new particle formation | atmosphere | fossil fuel

Airborne particles play an essential role in many serious environmental issues, including visibility reduction (1) and climate change (2), and have been linked to health problems associated with air pollution (3). On a global basis, sulfuric acid (H_2SO_4) is the most significant contributor to new particle formation in air, likely through reaction with ammonia and amines (4–6). In air, the dominant source for H_2SO_4 is the oxidation of SO_2 from combustion of sulfur-containing fossil fuels. Another source of new particle formation in air is the oxidation of organosulfur compounds (OSCs) generated by biological processes and agricultural activities (7–10). For example, oceans are a significant source of dimethyl sulfide (CH_3SCH_3, DMS) (10), whereas a variety of related species such as methanethiol (CH_3SH, MTO), dimethyl disulfide (CH_3SSCH_3, DMDS), and dimethyl trisulfide (CH_3SSSCH_3, DMTS) originate from livestock and farming practices (11–15). It has been shown that even human breath contains OSCs (16, 17). Atmospheric oxidation of OSCs generates not only SO_2 (which ultimately converts into H_2SO_4) but also methanesulfonic acid [$CH_3S(O)(O)OH$, MSA] (18), which also reacts with amines to generate new particles in air in the presence of water vapor (19, 20). Increasing regulations are driving the sulfur content and use of fossil fuels down (21), resulting in declining atmospheric SO_2 concentration and particulate sulfate concentrations. A key question for understanding future impacts of particles and for the development of cost-effective control policies is the extent to which atmospheric particulate matter can be controlled through regulation of fossil fuel combustion against a background of OSCs. We report here a distinctive multidisciplinary approach that integrates chemical mechanism development, quantum chemical calculations, field measurements, and 3D modeling to examine this issue in the context of a large, urban coastal area, the South Coast Air Basin of California (SoCAB).

Results and Discussion

The University of California Irvine–California Institute of Technology (UCI-CIT) model domain includes the Pacific Ocean on the west side, heavily populated urban areas, and an agricultural region with large cattle feedlots and associated sources around Chino, California, and constitutes the perfect domain for this study. The model includes spatially and temporally resolved emissions and typical meteorological conditions for this region, as well as a detailed chemical mechanism described as the 2005 base case (22). However, OSCs had not been included in this base case and some adjustments had to be made before running simulations (see *SI Appendix*, section 1 and Table S1 and discussion below for detailed OSC chemistry). First, the original emission rates of SO_2

Significance

Sulfur dioxide (SO_2) via its oxidation to sulfuric acid is a major source of airborne particles, which impact visibility, health, and climate. Sources of SO_2 include the combustion of sulfur-containing fossil fuels and the oxidation of organosulfur compounds (OSCs) such as dimethyl sulfide. We show that as fossil fuel combustion is phased out in an urban coastal area, particle formation will decrease substantially but still continue at a reduced rate due to the contribution from OSC oxidation products. Furthermore, methanesulfonic acid generated simultaneously in OSC oxidation will become a significant contributor to particle formation, which should be taken into account in predictive models of air pollution and climate and may be especially important in agricultural areas with significant OSC sources.

Author contributions: V.P., S.M., L.M.W., D.D., D.R.B., R.B.G., and B.J.F.-P. designed research; V.P., J.R.H., A.S.M., J.K., S.M., M.L.D., L.M.W., D.D., D.R.B., R.B.G., and B.J.F.-P. performed research; V.P., J.R.H., A.S.M., J.K., S.M., M.L.D., L.M.W., D.D., D.R.B., R.B.G., and B.J.F.-P. analyzed data; and V.P., J.R.H., A.S.M., J.K., S.M., M.L.D., L.M.W., D.D., R.B.G., and B.J.F.-P. wrote the paper.

The authors declare no conflict of interest.

This article is a PNAS Direct Submission.

[1]Present address: California Air Resources Board, Sacramento, CA 95814.

[2]To whom correspondence should be addressed. Email: bjfinlay@uci.edu.

This article contains supporting information online at www.pnas.org/lookup/suppl/doi:10.1073/pnas.1510743112/-/DCSupplemental.

and H_2SO_4 (3% of total anthropogenic SO_2 emitted) in the model (including emissions, boundary conditions, and initial conditions) were decreased by a factor of 4 compared with the 2005 base case to be consistent with the decrease in measured ambient SO_2 concentrations since 2005 (*SI Appendix*, section 1 and Fig. S1). This scenario is hereafter described as "representative of the year 2011–2013." A separate scenario was also run corresponding to a best-case futuristic scenario with no fossil fuel SO_2 (emissions, initial conditions, and boundary conditions all set to zero). For the scenario representative of the years 2011–2013, the boundary conditions include anthropogenic sources of SO_2 generated from Asia that are transported across the Pacific Ocean, emissions from ships in shipping lanes, along with sources from other states surrounding the SoCAB. In the zero anthropogenic SO_2 emissions scenario, those were turned off. Lastly, in the standard version of the model, H_2SO_4 partitions into existing particles or forms new particles if the concentrations exceed those for nucleation (23). However, significant uncertainties remain in quantitatively describing new particle formation from gas phase H_2SO_4 and MSA, especially given the recently recognized role of amines (4, 5). To compare the relative contributions of H_2SO_4 and MSA to new particle formation, nucleation and uptake into existing particles were turned off in the model to leave these species in the gas phase. We have shown in a previous study that under certain conditions, MSA and H_2SO_4 can form new particles at similar rates (20). As long as the processes such as reactions with amines that convert H_2SO_4 and MSA to new particles are similar for these two acids, their respective concentrations should provide an estimate of their potential relative contributions to new particle formation under different scenarios.

Second, three major contributors to OSCs were incorporated into the model: (*i*) oceanic emissions, (*ii*) agricultural activities, and (*iii*) urban sources. The first was captured by including a typical average emission flux for DMS of 10 μmol S m^{-2} d^{-1} in the summer months (10) in the model cells that encompass the coastal waters. Agriculture is a second potential source (11–15, 24–26). It was reported in previous studies that both NH_3 and OSC emissions are associated with livestock activities and that their concentrations were correlated (27, 28). Because emission flux measurements were not possible at the time for OSCs, we chose to estimate fluxes of OSCs from agricultural activities in the SoCAB by simultaneously measuring OSC and NH_3 ambient concentrations adjacent to a cattle feedlot in Chino, California (*SI Appendix*, sections 1 and 2) before dawn to avoid photochemistry. Fluxes for the OSCs were then estimated using the ratio of the measured concentrations in air to those of NH_3, whose emission fluxes are included in the base case of the model as indicated in *SI Appendix*, section 1 and Fig. S2. The average measured concentrations of DMS and DMDS were 1.2 ppb and 28 ppt, respectively, with a ratio of DMS to NH_3 concentrations of $(7.6 \pm 1.4) \times 10^{-3}$ and of DMDS to NH_3 of $(1.9 \pm 1.5) \times 10^{-4}$ (1 σ). Applying these to the nine model cells with agricultural activities around the Chino area yields emission fluxes of NH_3, DMS, and DMDS of 31, 0.24, and 5.8×10^{-3} μmol m^{-2} d^{-1}, respectively. Finally, heavily populated urban areas represent a third source, which includes emissions from human breath and pet waste. DMS was reported in human breath of healthy subjects at an average concentration of 13.8 ppb (17). The total volume of air inhaled and exhaled per day for an average person is 10,800 L (29), so that one person will typically emit 6.1 μmol of DMS per day. These human-associated emissions of DMS were incorporated into the model based on the population in each cell. Lastly, to assess the potential contribution from pets, measurements using proton-transfer mass spectrometry were made of the headspace of trash bins from a residential area where the bins are used mainly for pet waste. Methanethiol (MTO), DMS, and DMDS were unambiguously detected and quantified (*SI Appendix*, section 2, Fig. S3, and Tables S2 and S3). Emission fluxes were obtained by closing off the top of the container and measuring the increase in concentration of the OSCs with time. These were incorporated into the model on a basis proportional to population density. Potential emissions from other sources such as soils, vegetation (9), biomass burning (30), wetlands, and landfills, as well as emissions of other OSCs, such as hydrogen sulfide and carbonyl sulfide, were not included in the model because of the large uncertainties associated with their emissions estimates.

Third, although many of the individual steps have been established experimentally (18), surprisingly, the mechanism of production of MSA from OSC gas phase oxidation by hydroxyl radicals (OH, daytime) and nitrate radicals (nighttime) remains unclear (31). The $CH_3S(O)(O)O^{\bullet}$ free radical is likely the key intermediate (*SI Appendix*, section 3 and Fig. S4). The mechanism for the formation of MSA via hydrogen abstraction by $CH_3S(O)(O)O^{\bullet}$ from water and organic compounds, proposed earlier (18, 32, 33), were explored here using quantum chemical calculations. Results show that the ΔH for the $CH_3S(O)(O)O^{\bullet}$ + H_2O reaction is +6 kcal·mol^{-1}, consistent with earlier studies showing that the reverse reaction is exothermic (34). On the other hand, reactions of the $CH_3S(O)(O)O^{\bullet}$ radical with organic compounds such as formaldehyde (HCHO) or methane (CH_4) are more favorable. Fig. 1 shows that for HCHO, an initial complex (Min-3) is formed, which proceeds through transition state TS-2 and a second minimum Min-4 to form MSA and the HCO radical in what is essentially a barrierless reaction (*SI Appendix*, section 3, Fig. S5, and Table S4). Thus, hydrogen abstraction from aldehydes is fast and provides a feasible pathway to form MSA. As seen in Fig. 1, similar minima and transition states as for HCHO occur for the CH_4 reaction, but the energetics are not as favorable. Given that higher alkanes have weaker C–H bonds, this is a lower limit, and it may be that abstraction of a hydrogen atom from larger hydrocarbons can also contribute to MSA in air. These theoretical studies firmly establish that the mechanism of gas phase MSA formation is occurring via hydrogen abstraction from organics by the $CH_3S(O)(O)O^{\bullet}$ radical. This chemistry, detailed in *SI Appendix*, section 1 and Table S1, was incorporated into the UCI-CIT airshed model (22). Note that different mechanisms for DMS oxidation have been proposed previously (31, 33, 35–39). The intent of this study was to provide a reasonable mechanism for the oxidation of OSCs and to demonstrate that there are different non-fossil-fuel–related sources of sulfur compounds throughout the SoCAB that will remain as the dominant anthropogenic SO_2 emissions continue to decrease. As

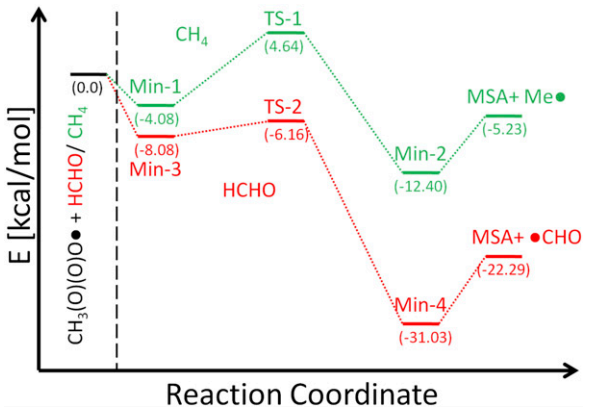

Fig. 1. Potential energy diagram for the reaction of $CH_3S(O)(O)O^{\bullet}$ radical with methane (CH_4) or formaldehyde (HCHO). See *SI Appendix*, section 3 for details of the theory applied.

such, the mechanism and rate constants were set based on the recommended chemistry and kinetics rate constants by Sander et al. (40), the IUPAC Task Group on Atmospheric Chemical Kinetic Data Evaluation (iupac.pole-ether.fr), and the current results from quantum chemical calculations.

Fig. 2 represents the hourly spatial distribution of both end products of the oxidation of OSCs—that is, H_2SO_4 and MSA. Suppressing the contribution from anthropogenic SO_2 emissions leads the domain-wide average concentrations of H_2SO_4 to decrease by a factor of 60 and the peak concentrations by a factor of 85 but not to zero, due to the continuing contribution from OSCs.

Each map corresponds to the predicted concentrations of each species during the third day of simulation, which reflects the combination of emissions of OSCs and anthropogenic SO_2 (for the case representative of 2011–2013), chemistry, and meteorology occurring during days 1, 2, and into day 3. First, although MSA is produced solely by oxidation of OSCs (no direct emissions), H_2SO_4 is partly emitted from direct emissions associated with fossil fuel combustion (as 3% of SO_2 according to the 2005 baseline emission inventory) under the conditions representative of 2011–2013 and is also produced from SO_2 oxidation. As a result, in the early morning of day 3, the H_2SO_4 peak maximum is observed around the ports of Long Beach in the scenario representative of 2011–2013 (Fig. 2*A*), reflecting the direct emissions. As the day proceeds, the air mass flows northeast (NE), leading to dilution and transport of the H_2SO_4 plume further inland, while at the same time, SO_2 is being converted to H_2SO_4. In addition, a second hot spot of H_2SO_4 is observed north of Riverside in the early morning, which corresponds to the residual H_2SO_4 that has been produced and transported during the previous days. This behavior is typical of the SoCAB and is due to the sea breeze flowing inland in a NE direction during the day (6:00–20:00 h) and back at night, which typically concentrates airborne pollutants in that region of the domain (22). In the zero emissions scenario (Fig. 2*B*), the observed spatial distribution of H_2SO_4 is quite different. In this scenario, the peak maximum for H_2SO_4 originates solely from chemistry (oxidation of OSCs forming SO_2 that is then converted into H_2SO_4) and meteorology. The hot spot observed early in the morning is primarily due to the residual H_2SO_4 (and SO_2) formed and transported from the previous days of simulation. The fresh formation of both SO_2 and H_2SO_4 following the oxidation of oceanic DMS is observed later during the day, due to the relatively slow reaction. The DMS plume formed close to the coast where the highest source is found is driven inland following the sea breeze path. This is visible in Fig. 3*C*, where the DMS concentration falls during the morning due to both dilution and reaction with OH. Under a typical daytime OH concentration of 5×10^6 cm^{-3}, the DMS lifetime is about ∼8 h, whereas that for the SO_2 to H_2SO_4 conversion is relatively slow (∼2 d at an OH concentration of 5×10^6 cm^{-3}), which results in somewhat different geographical and temporal distributions for H_2SO_4 and SO_2 as the air mass evolves throughout the day. For example, the domain-wide peak maximum for SO_2 occurs at 6:00 h, whereas the domain-wide peak maximum for H_2SO_4 is observed much later during the day, at around 14:00 h, but also at a different area of the domain as the air mass has traveled.

Fig. 2*C* shows contours for gas phase MSA formed in the DMS oxidation. The chemistry forming MSA occurs faster than the conversion of SO_2 to H_2SO_4. Once formed, the spatial distribution of MSA is predominantly governed by meteorology. In the zero SO_2/H_2SO_4 emissions scenario, although both MSA and SO_2 are derived from the oxidation of OSCs, their distribution in the SoCAB is different (Figs. 2*C* and 3*B*). This result is not

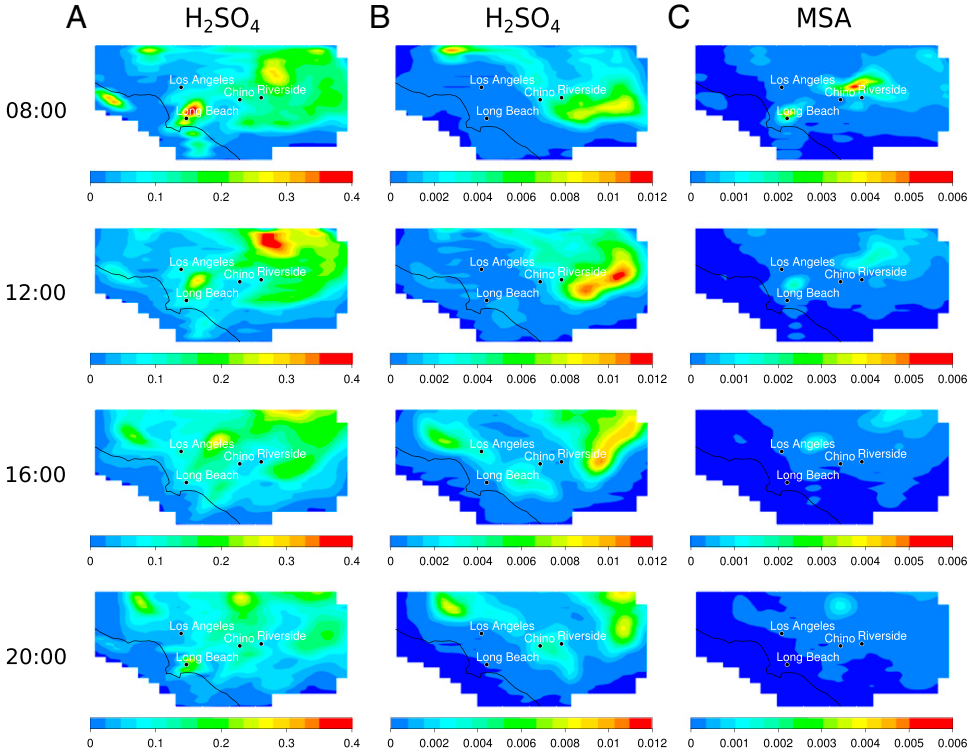

Fig. 2. Model-predicted gas phase H_2SO_4 and MSA concentrations (ppb) in the SoCAB at 8:00 h, 12:00 h, 16:00 h, and 20:00 h. (*A*) H_2SO_4 concentrations (ppb) with SO_2 and H_2SO_4 emissions representative of 2011–2013. (*B*) H_2SO_4 concentrations (ppb) with sulfur fossil fuel emissions, boundary conditions, and initial conditions for SO_2 and H_2SO_4 set to zero. (*C*) MSA concentrations (ppb) with sulfur fossil fuel emissions, boundary conditions, and initial conditions for SO_2 and H_2SO_4 set to zero. The domain-wide average gas phase MSA concentration is not significantly sensitive to the scenario chosen for sulfur fossil fuel emissions.

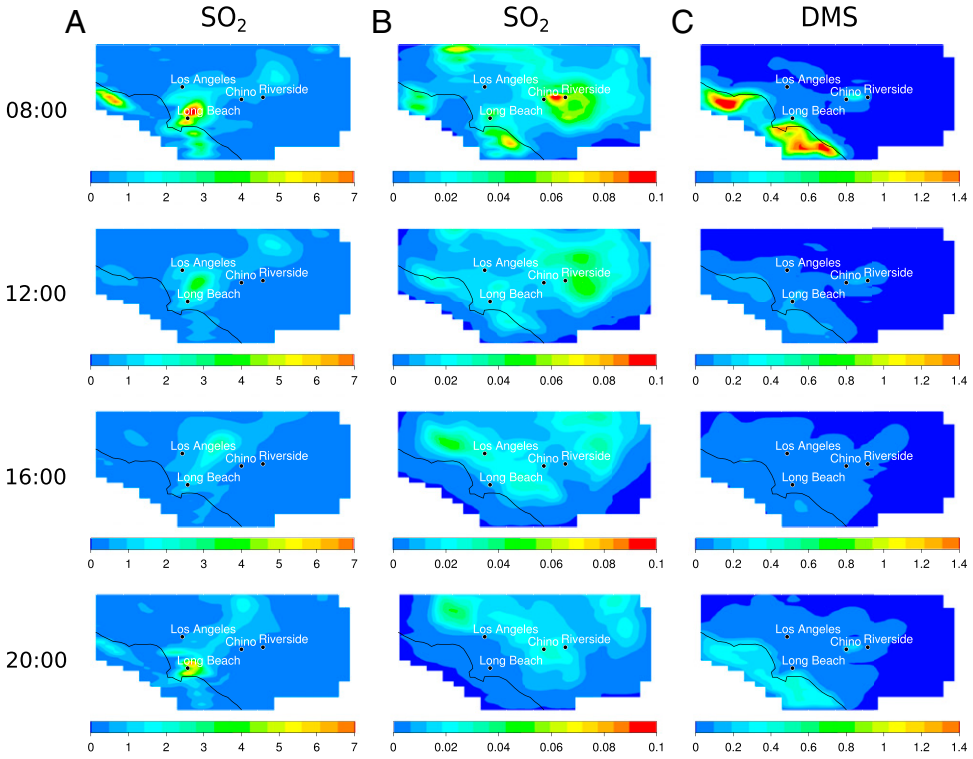

Fig. 3. Model-predicted gas phase SO_2 and DMS concentrations (ppb) in the SoCAB at 08:00 h, 12:00 h, 16:00 h, and 20:00 h with urban, agriculture, and ocean OSCs emission sources included. (*A*) SO_2 concentrations (ppb) with SO_2 and H_2SO_4 emissions representative of 2011–2013. (*B*) SO_2 concentrations (ppb) with sulfur fossil fuel emissions, boundary conditions, and initial conditions for SO_2 and H_2SO_4 set to zero. (*C*) DMS concentrations (ppb) with sulfur fossil fuel emissions, boundary conditions, and initial conditions for SO_2 and H_2SO_4 set to zero.

surprising. As described in the mechanism (*SI Appendix*, section 3 and Fig. S4), MSA formation is particularly influenced by NO_x. A positive correlation between MSA formation and NO_x concentration has been previously reported in laboratory experiments (41). Thus, fresh MSA is formed once the DMS plume encounters enough NO_x for the reactions to occur, such as the ports located around Long Beach, as well as urban areas further inland (*SI Appendix*, section 4 and Fig. S6). This explains why the SO_2 distribution largely follows the DMS plume contour, whereas MSA is present in more localized and concentrated areas associated with higher NO_x concentrations. Again, a second hot spot can be seen north of Riverside, which is the residual from the chemistry and meteorology occurring during days 1 and 2. In brief, the localized hot spots for the different species are governed by the emissions, chemistry, and the unique meteorology of the domain.

To investigate the relative source strengths of OSCs, the respective source contributions for DMS are presented in Fig. 4, which indicates the magnitude of the different contributions as well as differences in the spatial distributions of the three types of sources. Results for DMS are presented here as a representative for OSCs, as it is the more abundant species emitted. Fig. 4 clearly shows that the OSCs produced from the ocean overwhelm the other contributions (peak maximum DMS predicted at 1.4 ppb). Agricultural activities also contribute significantly to the total DMS emitted, with up to about a third of the total DMS peak maximum concentration observed from this source localized around the Chino/Riverside area. Urban emissions alone produce a peak maximum DMS concentration of only 0.1% of that seen from oceanic sources. For completeness, corresponding source-specific predicted concentrations for MSA, SO_2, and H_2SO_4 are presented in *SI Appendix*, Figs. S7–S9 (*SI Appendix*, section 4), respectively.

Ambient submicron particle measurements were made with a high-resolution time-of-flight aerosol mass spectrometer (AMS) at the north campus of the University of California Irvine, which is located in the SoCAB approximately 5 miles inland from the Pacific Ocean. Peaks typical of OSCs were observed on many days; *SI Appendix*, section 5 and Fig. S10 show an average mass spectrum of the OSC-specific ion signals identified by high resolution and clearly shows the presence of high-intensity peaks at *m/z* 78, 79, and 96 corresponding to $CH_2SO_2^+$, $CH_3SO_2^+$, and $CH_4SO_3^+$, respectively, which are characteristic of MSA (42). Some of these days also show the presence of peaks typical of sea salt chloride. Fig. 5 shows data in which NaCl and MSA are correlated in some cases (Fig. 5*A*) and uncorrelated in others (Fig. 5*B*), suggesting that nonoceanic sources of MSA can also be important in this location, despite its proximity to the Pacific Ocean. Previous reports of MSA in particles in Riverside, California were attributed to oxidation of oceanic emissions during transport (43). On the other hand, measurements of MSA in particles in the Central Valley of California, a major agricultural area, were reported to be independent of transport from the coast (42). This finding is in good agreement with our results, indicating that continental sources, especially from agricultural activities, may be significant sources for MSA. Results from this study have particular significance for future air quality in agricultural regions where emissions of OSCs can be much higher than those indicated by the measurements in the current study. For example, *SI Appendix*, section 6 and Fig. S11 show DMS in and around a dairy located in the Central Valley (about 28 miles south of Fresno, California), with levels within the dairy itself up to 12 ppb. Exploring alternative agricultural practices that minimize such emissions and their impacts on air quality, visibility, health, and climate may be prudent in such areas in the future.

In summary, removing anthropogenic SO_2 emissions from a large coastal urban area causes MSA to become relatively more important as a particle source and does not decrease H_2SO_4 to zero. For

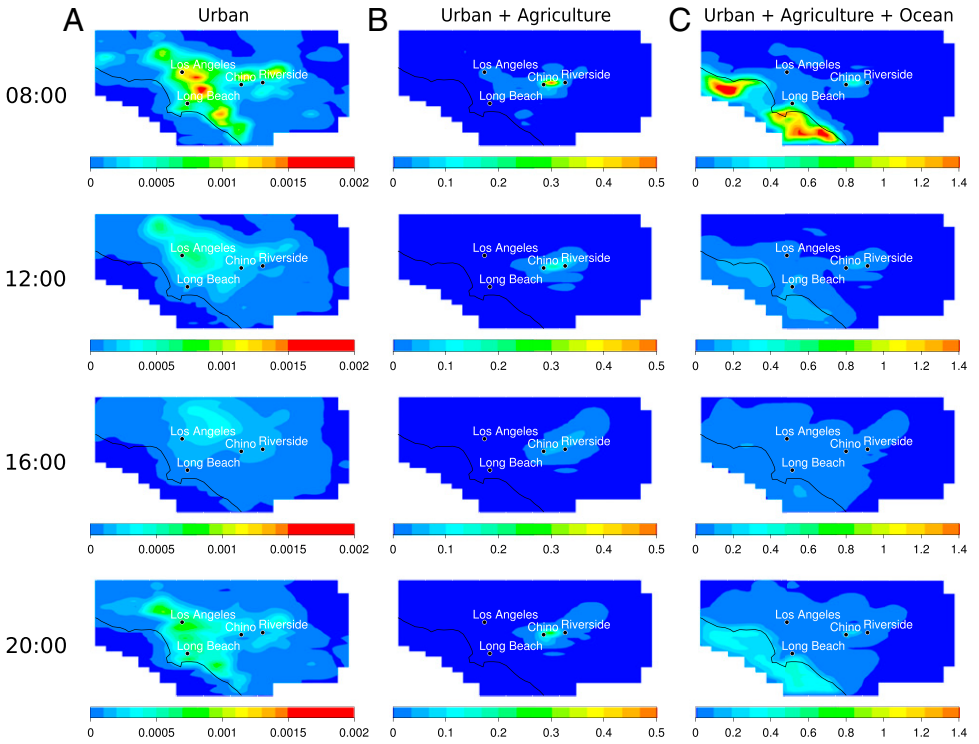

Fig. 4. Model-predicted gas phase DMS concentrations (ppb) at 08:00 h, 12:00 h, 16:00 h, and 20:00 h with sulfur fossil fuel emissions, boundary conditions, and initial conditions for SO_2 and H_2SO_4 set to zero. (*A*) Only urban OSC emission sources including DMS emissions from humans and DMS, DMDS, and MTO from pet waste. (*B*) Urban and agriculture OSC emission sources (same conditions as *A* plus DMS and DMDS emissions from Chino, California). (*C*) Urban, agriculture, and ocean OSC emission sources (same conditions as *B* plus DMS from ocean).

example, the ratio of domain-wide average concentrations of MSA/H_2SO_4 changes from 0.005 for the 2011–2013 case to 0.24 for the zero fossil fuel emissions case. Note, however, that these are likely to be lower limits to the MSA/H_2SO_4 ratio for the 2011–2013 scenario, as OSC emissions from wetlands, soils, vegetation, and so forth have not been included. Because H_2SO_4 and MSA are known precursors to new particles, the number concentration of particles should also decrease significantly, as long as scavenging by existing particles is not important. The predicted 21 ppt and 14 ppt peak concentrations of MSA and H_2SO_4 observed, respectively, at 06:00 h and 14:00 h correspond to mass concentrations of only 0.08 $\mu g \cdot m^{-3}$ and 0.06 $\mu g \cdot m^{-3}$, respectively, well below current air quality standards for $PM_{2.5}$. However, because of its acidity, H_2SO_4 (and potentially MSA) can enhance the formation and growth of secondary organic aerosol (SOA) from organic compounds (5, 44, 45), including those produced by homogeneous nucleation of low-volatility species (46). This process would result in higher particle mass concentrations than those predicted based on the acids alone. The importance of this process is not clear in the SoCAB as amines and ammonia are always present, especially in agriculture areas where they will neutralize the sulfur-containing acid, forming ammonium (or aminium) sulfate salt particles. On the other hand, ammonium sulfate has also been shown to react in particles to yield light-absorbing "brown" carbon (47–49).

Materials and Methods

Details of the experimental, theoretical, and modeling approaches are found in *SI Appendix*. Quantum chemical calculations were carried out to determine the energy barriers and total energetics of potential reactions of the $CH_3S(O)(O)O^{\bullet}$ radical to form MSA. The CCSD(T) method used with Dunning's cc-pV(T+d)Z basis set (50, 51) along with the restricted open-shell approach as implemented in Molpro package (52) was applied to optimize geometries of isolated species. Complexes and transition states were optimized using the multiconfigurational self-consistent field (MCSCF) method. Single point calculations using the CCSD(T)/cc-pV(T+d)Z method were performed to obtain energies for reaction profiles. The harmonic approximation with the CCSD(T)/cc-pV(T+d)Z method was used to estimate thermodynamic values for the structures.

The atmospheric model calculations were performed using the UCI-CIT regional airshed model (22). The meteorological conditions were identical in all runs and were taken from August 27–29, 1987, for which the model has been tested previously (22, 53–55) and which represent an ideal set of conditions for modeling a pollution episode (22). The 2005 baseline emissions inventory documented in the 2007 Air Quality Management Plan formulated by the South Coast Air Quality Management District (56) was used for all species, except SO_2/H_2SO_4. Emission rates of all species present in the inventory, including NO_x, are kept constant for each run, with the exception of SO_2/H_2SO_4, as described earlier. Emissions of MTO, DMS, and DMDS from various sources obtained from the literature (10, 17) or from direct measurements as detailed in *SI Appendix*, section 2 were incorporated into the model.

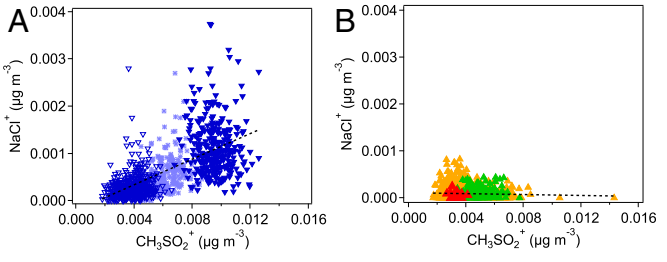

Fig. 5. Plots of $Na^{35}Cl^+$ ion versus MSA ion ($CH_3SO_2^+$). (*A*) NaCl and MSA are correlated (overall r^2 = 0.41) for (light blue ⋆) August 2, 2012 (9:15–14:20), (dark blue ▽) August 27, 2012 (10:00–20:05), and (dark blue ▼) August 31, 2012 (10:20–16:50). (*B*) NaCl and MSA are uncorrelated (overall r^2 = 0.0023) for (orange ▲) July 28, 2010 (10:10)–July 29, 2010 (15:00), (green ▲) May 14, 2012 (10:35–13:55), and (red ▲) August 26, 2014 (13:50–14:05). Measurements were made in Irvine, California. Mass loading for NaCl is uncorrected for its low sensitivity in the AMS due to inefficient vaporization. Data points represent 1–2-min sampling times. Dashed lines are linear fits to all data points in each plot.

In addition, a detailed oxidation mechanism for OSCs was added to the model (*SI Appendix*, sections 1 and 3), including reactions of the $CH_3S(O)(O)O^{\bullet}$ radical with HCHO and larger aldehydes.

Measurements of gas phase OSCs were made using high-resolution time-of-flight proton transfer mass spectrometry (PTR-ToF-MS 8000, Ionicon Analytik) (57, 58) and gas chromatography coupled with flame ionization detector (Hewlett Packard 6890) of air samples collected in electropolished stainless steel canisters (59). MSA and markers for sea salt in ambient particles were measured using a high-resolution time-of-flight AMS (Aerodyne) (60).

ACKNOWLEDGMENTS. The authors appreciate helpful discussions with E. Saltzman and technical assistance from B. Love, B. Barletta, and J. Marrero. The authors are grateful to the National Science Foundation (Grants 0909227, 0923323, 1443140, and 1337080) and the Department of Energy (Grant ER65208) for support of this work.

1. Finlayson-Pitts BJ, Pitts JN, Jr (2000) *Chemistry of the Upper and Lower Atmosphere—Theory, Experiments, and Applications* (Academic Press, San Diego, CA), p 969.
2. IPCC (2013) *Summary for Policymakers in Climate Change* (Press CU, Cambridge, UK).
3. Pope CA, 3rd, Dockery DW (2006) Health effects of fine particulate air pollution: Lines that connect. *J Air Waste Manag Assoc* 56(6):709–742.
4. Smith JN, et al. (2010) Observations of aminium salts in atmospheric nanoparticles and possible climatic implications. *Proc Natl Acad Sci USA* 107:6634–6639.
5. Zhang R, Khalizov A, Wang L, Hu M, Xu W (2012) Nucleation and growth of nanoparticles in the atmosphere. *Chem Rev* 112(3):1957–2011.
6. Sipilä M, et al. (2010) The role of sulfuric acid in atmospheric nucleation. *Science* 327(5970):1243–1246.
7. Aneja VP (1990) Natural sulfur emissions into the atmosphere. *J Air Waste Manage Assoc* 40(4):469–476.
8. Bates TS, Lamb BK, Guenther A, Dignon J, Stoiber RE (1992) Sulfur emissions to the atmosphere from natural sources. *J Atmos Chem* 14(1-4):315–337.
9. Jardine K, et al. (2015) Dimethylsulfide in the Amazon rainforest. *Global Biogeochem Cycles* 29(1):19–32.
10. Lana A, et al. (2011) An updated climatology of surface dimethlysulfide concentrations and emission fluxes in the global ocean. *Global Biogeochem Cycles* 25(1): BG1004.
11. Hansen MJ, Toda K, Obata T, Adamsen APS, Feilberg A (2012) Evaluation of single column trapping/separation and chemiluminescence detection for measurement of methanethiol and dimethyl sulfide from pig production. *J Anal Methods Chem* 2012: 489239.
12. Filipy J, Rumburg B, Mount G, Westberg H, Lamb B (2006) Identification and quantification of volatile organic compounds from a dairy. *Atmos Environ* 40(8):1480–1494.
13. Feilberg A, Liu D, Adamsen APS, Hansen MJ, Jonassen KEN (2010) Odorant emissions from intensive pig production measured by online proton-transfer-reaction mass spectrometry. *Environ Sci Technol* 44(15):5894–5900.
14. Trabue S, et al. (2008) Field sampling method for quantifying volatile sulfur compounds from animal feeding operations. *Atmos Environ* 42(10):3332–3341.
15. Rumsey IC, Aneja VP, Lonneman WA (2014) Characterizing reduced sulfur compounds emissions from a swine concentrated animal feeding operation. *Atmos Environ* 94:458–466.
16. Suarez FL, Furne JK, Springfield J, Levitt MD (2000) Morning breath odor: Influence of treatments on sulfur gases. *J Dent Res* 79(10):1773–1777.
17. Van den Velde S, Nevens F, Van Hee P, van Steenberghe D, Quirynen M (2008) GC-MS analysis of breath odor compounds in liver patients. *J Chromatogr B Analyt Technol Biomed Life Sci* 875(2):344–348.
18. Barnes I, Hjorth J, Mihalopoulos N (2006) Dimethyl sulfide and dimethyl sulfoxide and their oxidation in the atmosphere. *Chem Rev* 106(3):940–975.
19. Chen H, et al. (2015) New particle formation and growth from methanesulfonic acid, trimethylamine and water. *Phys Chem Chem Phys* 17(20):13699–13709.
20. Dawson ML, et al. (2012) Simplified mechanism for new particle formation from methanesulfonic acid, amines, and water via experiments and *ab initio* calculations. *Proc Natl Acad Sci USA* 109(46):18719–18724.
21. Stern DI (2005) Global sulfur emissions from 1850 to 2000. *Chemosphere* 58(2):163–175.
22. Carreras-Sospedra M, Dabdub D, Rodríguez M, Brouwer J (2006) Air quality modeling in the South Coast Air Basin of California: What do the numbers really mean? *J Air Waste Manag Assoc* 56(8):1184–1195.
23. Wexler AS, Lurmann FW, Seinfeld JH (1994) Modeling urban and regional aerosols. 1. Model development. *Atmos Environ* 28(3):531–546.
24. Shaw SL, et al. (2007) Volatile organic compound emissions from dairy cows and their waste as measured by proton-transfer-reaction mass spectrometry. *Environ Sci Technol* 41(4):1310–1316.
25. Hobbs P, Mottram T (2000) Significant contributions of dimethyl sulphide from livestock to the atmosphere. *Atmos Environ* 34(21):3649–3650.
26. Williams J, et al. (1999) Atmospheric methyl halides and dimethyl sulfide from cattle. *Geophys Res Lett* 13(2):485–491.
27. Hobbs PJ, Webb J, Mottram TT, Grant B, Misselbrook TM (2004) Emissions of volatile organic compounds originating from UK livestock agriculture. *J Sci Food Agric* 84(11):1414–1420.
28. Blanes-Vidal V, Hansen MN, Sousa P (2009) Reduction of odor and odorant emissions from slurry stores by means of straw covers. *J Environ Qual* 38(4):1518–1527.
29. Phalen RF (1984) *Inhalation Studies: Foundations and Techniques* (CRC Press, Boca Raton, FL).
30. Meinardi S, Simpson IJ, Blake NJ, Blake DR, Rowland FS (2003) Dimethyl disulfide (DMDS) and dimethyl sulfide (DMS) emissions from biomass burning in Australia. *Geophys Res Lett* 30(9):1454.
31. Karl M, Gross A, Leck C, Pirjola L (2007) Intercomparison of dimethylsulfide oxidation mechanisms for the marine boundary layer: Gaseous and particulate sulfur constituents. *J Geophys Res* 112(D15):D15304.
32. Hatakeyama S, Akimoto H (1983) Reactions of OH radicals with methanethiol, dimethylsulfide and dimethyl disulfide in air. *J Phys Chem* 87(13):2387–2395.
33. Yin FD, Grosjean D, Seinfeld JH (1990) Photoxidation of dimethyl sulfide and dimethyl disulfide. I: Mechanism development. *J Atmos Chem* 11(4):309–364.
34. Jørgensen S, Jensen C, Kjaergaard HG, Anglada JM (2013) The gas-phase reaction of methane sulfonic acid with the hydroxyl radical without and with water vapor. *Phys Chem Chem Phys* 15(14):5140–5150.
35. Berndt T, Richters S (2012) Products of the reaction of OH radicals with dimethyl sulphide in the absence of NOx: Experiment and simulation. *Atmos Environ* 47:316–322.
36. Yin FD, Grosjean D, Flagan RC, Seinfeld JH (1990) Photooxidation of dimethyl sulfide and dimethyl disulfide. 2: Mechanism evaluation. *J Atmos Chem* 11(4):365–399.
37. Koga S, Tanaka H (1999) Modeling the methanesulfonate to non-sea-salt sulfate molar ratio and dimethylsulfide oxidation in the atmosphere. *J Geophys Res* 104(D11): 13735–13747.
38. Lucas DD, Prinn RG (2002) Mechanistic studies of dimethylsulfide oxidation products using an observationally constrained model. *J Geophys Res* 107(D14):Artn 4201.
39. Capaldo KP, Pandis SN (1997) Dimethylsulfide chemistry in the remote marine atmosphere: Evaluation and sensitivity analysis of available mechanisms. *J Geophys Res* 102(D19):23251–23267.
40. Sander SP, et al. (2011) *Chemical Kinetics and Photochemical Data for Use in Atmospheric Studies. Evaluation Number 17*, JPL Publication (Jet Propulsion Laboratory, Pasadena, CA), Vol 10-6. Available at jpldataeval.jpl.nasa.gov. Accessed August 12, 2015.
41. Patroescu IV, Barnes I, Becker KH, Mihalopoulos N (1999) FT-IR product study of the OH-initiated oxidation of DMS in the presence of NOx. *Atmos Environ* 33(1):25–35.
42. Ge X, Zhang Q, Sun Y, Ruehl CR, Setyan A (2012) Effect of aqueous-phase processing on aerosol chemistry and size distributions in Fresno, California, during wintertime. *Environ Chem* 9(3):221–235.
43. Gaston CJ, Pratt KA, Qin X, Prather KA (2010) Real-time detection and mixing state of methanesulfonate in single particles at an inland urban location during a phytoplankton bloom. *Environ Sci Technol* 44(5):1566–1572.
44. Hallquist M, et al. (2009) The formation, properties and impact of secondary organic aerosol: Current and emerging issues. *Atmos Chem Phys* 9(14):5155–5236.
45. Xu L, et al. (2015) Effects of anthropogenic emissions on aerosol formation from isoprene and monoterpenes in the southeastern United States. *Proc Natl Acad Sci USA* 112(1):37–42.
46. Ehn M, et al. (2014) A large source of low-volatility secondary organic aerosol. *Nature* 506(7489):476–479.
47. Powelson MH, Espelien BM, Hawkins LN, Galloway MM, De Haan DO (2014) Brown carbon formation by aqueous-phase carbonyl compound reactions with amines and ammonium sulfate. *Environ Sci Technol* 48(2):985–993.
48. Laskin A, Laskin J, Nizkorodov SA (2015) Chemistry of atmospheric brown carbon. *Chem Rev* 115(10):4335–4382.
49. Nguyen TB, et al. (2012) Formation of nitrogen- and sulfur-containing light-absorbing compounds accelerated by evaporation of water from secondary organic aerosols. *J Geophys Res* 117:D01207.
50. Dunning TH (1989) Gaussian-basis sets for use in correlated molecular calculations. 1. The atoms boron through neon and hydrogen. *J Chem Phys* 90(2):1007–1023.
51. Dunning TH, Peterson KA, Wilson AK (2001) Gaussian basis sets for use in correlated molecular calculations. X. The atoms aluminum through argon revisited. *J Chem Phys* 114(21):9244–9253.
52. Werner H-J, et al. (2012) MOLPRO, Version 2012, a Package for ab Initio Programs. Available at www.molpro.net. Accessed August 12, 2015.
53. Nguyen K, Dabdub D (2002) NOx and VOC control and its effects on the formation of aerosols. *Aerosol Sci Technol* 36(5):560–572.
54. Carreras-Sospedra M, Vutukuru S, Brouwer J, Dabdub D (2010) Central power generation versus distributed generation—An air quality assessment in the South Coast Air Basin of California. *Atmos Environ* 44(26):3215–3223.
55. Chang WL, Griffin RJ, Dabdub D (2010) Partitioning phase preference for secondary organic aerosol in an urban atmosphere. *Proc Natl Acad Sci USA* 107(15):6705–6710.
56. SCAQMD (2007) *Air Quality Management Plan (AQMP) (Air Quality Management District (AQMD))*. Available at www.aqmd.gov/home/library/clean-air-plans/air-quality-mgt-plan/2007-air-quality-management-plan. Accessed January 2015.
57. Graus M, Müller M, Hansel A (2010) High resolution PTR-TOF: Quantification and formula confirmation of VOC in real time. *J Am Soc Mass Spectrom* 21(6):1037–1044.
58. Jordan A, et al. (2009) A high resolution and high sensitivity proton-transfer-reaction time-of-flight mass spectrometer (PTR-TOF-MS). *Int J Mass Spectrom* 286(2-3):122–128.
59. Colman JJ, et al. (2001) Description of the analysis of a wide range of volatile organic compounds in whole air samples collected during PEM-tropics A and B. *Anal Chem* 73(15):3723–3731.
60. DeCarlo PF, et al. (2006) Field-deployable, high-resolution, time-of-flight aerosol mass spectrometer. *Anal Chem* 78(24):8281–8289.